Toward unlocking the Mn^{3+}/Mn^{2+} redox pair in alluaudite-type $Na_{2+2z}Mn_{2-z}(SO_4)_{3-x}(SeO_4)_x$ cathodes for sodium-ion batteries

Accepted Manuscript

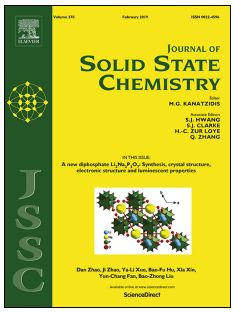

Toward unlocking the Mn^{3+}/Mn^{2+} redox pair in alluaudite-type $Na_{2+2z}Mn_{2-z}(SO_4)_{3-x}(SeO_4)_x$ cathodes for sodium-ion batteries

Maria A. Kirsanova, Dries De Sloovere, Olesia M. Karakulina, Joke Hadermann, Marlies K. Van Bael, An Hardy, Artem M. Abakumov

PII: S0022-4596(19)30366-4

DOI: https://doi.org/10.1016/j.jssc.2019.07.032

Reference: YJSSC 20871

To appear in: *Journal of Solid State Chemistry*

Received Date: 4 June 2019

Revised Date: 17 July 2019

Accepted Date: 17 July 2019

Please cite this article as: M.A. Kirsanova, D. De Sloovere, O.M. Karakulina, J. Hadermann, M.K. Van Bael, A. Hardy, A.M. Abakumov, Toward unlocking the Mn^{3+}/Mn^{2+} redox pair in alluaudite-type $Na_{2+2z}Mn_{2-z}(SO_4)_{3-x}(SeO_4)_x$ cathodes for sodium-ion batteries, *Journal of Solid State Chemistry* (2019), doi: https://doi.org/10.1016/j.jssc.2019.07.032.

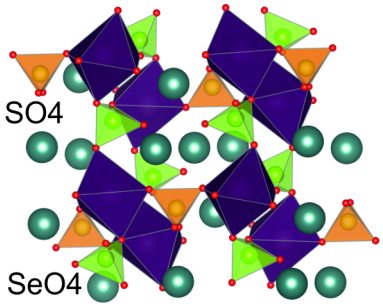

Toward unlocking the Mn^{3+}/Mn^{2+} redox pair in alluaudite-type $Na_{2+2z}Mn_{2-z}(SO_4)_{3-x}(SeO_4)_x$ cathodes for sodium-ion batteries

Maria A. Kirsanova,[1,a,*] Dries De Sloovere,[2,3,a] Olesia M. Karakulina,[4] Joke Hadermann,[4] Marlies K. Van Bael,[2,3] An Hardy,[2,3] Artem M. Abakumov[1]

[a] Equal contribution

[1] Skolkovo Institute of Science and Technology, Nobel str. 3, 143026 Moscow, Russia

[2] Institute for Materials Research (IMO-imomec), UHasselt, Martelarenlaan 42, B-3500 Hasselt, Belgium

[3] Energyville, Thor Park 8320, B-3600 Genk, Belgium

[4] EMAT, University of Antwerp, Groenenborgerlaan 171, B-2020 Antwerpen, Belgium

*corresponding author: m.kirsanova@skoltech.ru

Abstract

In polyanion cathodes, the inductive effect alters the potential of a $M^{(n+1)+}/M^{n+}$ redox couple (M – transition metal) according to the electronegativity of the X cation in the polyanion groups (XO_4^{m+}). To manipulate the operating potential, we synthesized a series of mixed sulfate-selenate alluaudites, with structure formulas $Na_{2+2z}Mn_{2-z}(SO_4)_{3-x}(SeO_4)_x$ and $Na_{2.81}Ni_{1.60}(SO_4)_{1.43}(SeO_4)_{1.57}$. Their crystal structure was determined from powder X-ray diffraction data, revealing that the Mn-based alluaudites form solid solutions with the same crystal structure for x = 0.75; 1.125 and 1.5. $Na_{2.81}Ni_{1.60}(SO_4)_{1.43}(SeO_4)_{1.57}$ is isostructural to the Mn-based alluaudites. Although the $Na_{2+2z}Mn_{2-z}(SO_4)_{3-x}(SeO_4)_x$ compound with the highest selenium content demonstrates a reversible discharge capacity of 60 mAh g^{-1}, only a small part of this electrochemical activity can be ascribed to the Mn^{3+}/Mn^{2+} redox couple. The redox potential of the Mn^{3+}/Mn^{2+} pair in $Na_{2+2z}Mn_{2-z}(SO_4)_{3-x}(SeO_4)_x$ decreases with increasing values of x, in agreement with the lower electronegativity of Se compared to that of S.

Keywords

Crystal structure, Inductive effect, Polyanion compounds, Na-ion cathode materials

1. Introduction

Besides the electronegativity, ionization energy, electronic configuration and oxygen coordination of the transition metal cation M, the redox potential of the $M^{(n+1)+}/M^{n+}$ pair in polyanion positive electrode (cathode) materials for metal-ion batteries depends on the inductive effect. This effect originates from a competition for electron density between M^{n+} and the highly charged X^{m+} cation in the M-O-X bonds, in which the oxygen atom is part of both a MO_6 octahedral unit and a XO_4/XO_3 polyanion group (such as phosphate, sulfate, silicate, carbonate, borate, etc.). A higher electronegativity of the X^{m+} cation increases the ionicity of the M-O bond and therefore raises the potential of the $M^{(n+1)+}/M^{n+}$ redox pair [1,2]. For lithium-ion battery (LIB) cathodes, the dependence of the $M^{(n+1)+}/M^{n+}$ redox potential on the electronegativity of X^{m+} has been exemplified systematically in $Li_xFe_2(XO_4)_3$ (with X = As, P, Mo, W, S) [3–5]. Similar trends were observed for $LiCoXO_4$ (X = P, As) [6] and Li_yVOXO_4 (X = P, As, Si, Ge) [7], where the potential of Li^+ deintercalation increases linearly with the Mulliken electronegativity of X^{m+} within the GeO_4<SiO_4<PO_4 row.

Although not studied as comprehensively as in their LIB counterparts, the inductive effect also appears as an important factor affecting the electrochemical potential in sodium-ion battery (SIB) cathodes. For instance, for the Fe^{3+}/Fe^{2+} redox couple, the average sodium deintercalation potential generally follows the trend of increasing electronegativity of X^{m+} in the series of silicates (Na_2FeSiO_4: 1.6–1.9 V *vs*. Na^+/Na) [8] – phosphates ($NaFePO_4$: 2.8 V *vs*. Na^+/Na [9] $Na_2Fe_3(PO_4)_3$: 2.7 V *vs*. Na^+/Na) [10] – sulfates ($Na_2Fe(SO_4)_2$: 3.4 V *vs*. Na^+/Na) [11,12]. Among the iron-based SIB cathodes, the highest-ever reported Fe^{3+}/Fe^{2+} redox potential (at 3.8 V *vs*. Na^+/Na) has been demonstrated by Barpanda *et al.* in $Na_2Fe_2(SO_4)_3$, which adopts an alluaudite-type structure [13]. Alluaudite-type $Na_{2+2x}Fe_{2-x}(SO_4)_3$ compounds form open frameworks, which results in excellent kinetics of the sodium ion deintercalation and good structural stability. It is tempting to prepare alluaudites with other 3d metal M^{3+}/M^{2+} (M = Mn, Co, Ni) redox pairs and investigate their electrochemical properties, but for M = Mn, the sodium deintercalation potential is prohibitively high in phosphates, and even more so in sulfates. Therefore, in alluaudite-type $Na_2Fe_{3-x}Mn_x(PO_4)_3$ solid solutions, the deintercalation of sodium ions is solely attributed to the redox reaction of the Fe^{3+}/Fe^{2+} pair [10]. The activation of the

Mn^{3+}/Mn^{2+} redox pair in the alluaudite framework was possible only with the replacement of phosphate/sulfate groups with molybdate groups, which have a significantly lower electronegativity. This resulted in the formation of $Na_{2.67}Mn_{1.67}(MoO_4)_3$, with an average sodium ion deintercalation potential 3.45 V *vs*. Na^+/Na [14]. Some electrochemical activity is reported for alluaudite-type $Na_{2.44}Mn_{1.78}(SO_4)_3$ as LIB cathode. This, however, requires several activation cycles with charging up to 4.7 V *vs*. Li^+/Li, and the nature of this activation is not yet fully understood [15].

Recently, Driscoll *et al.* [16] reported on a series of the alluaudite compounds $Na_2M(SO_4)_{2-x}(SeO_4)_x$ (M = Mn, Co, Ni; $0 \leq x \leq 1$). For M = Mn, phase-pure alluaudite phases were formed across the whole compositional range, whereas for M = Co and M = Ni, phase-pure samples were synthesized only for $x \geq 0.5$ and $x = 1$, respectively. The complete range of $Na_2Mn(SO_4)_{2-x}(SeO_4)_x$ solid solutions provides an excellent opportunity to tune the sodium ion deintercalation potential and to study the effect of the substitution of less electronegative SeO_4^{2-} groups for SO_4^{2-} (the Milliken electronegativities of S and Se are 2.651 and 2.509, respectively) [17]. Here, we report on the synthesis, crystal structure refinement and electrochemical behaviour of the Mn- and Ni-based Se-substituted alluaudites as novel high-voltage SIB cathodes and demonstrate the unlocking of the Mn^{3+}/Mn^{2+} redox pair by tuning the redox potential through substitution of SO_4^{2-} by SeO_4^{2-}, in line with the inductive effect. However, only a minor part of the total electrochemical activity could be attributed to this redox pair and the additional capacity may originate from the Se^{6+}/Se^{4+} couple.

2. Experimental

2.1. Synthesis

The samples were synthesized by dissolving $MnSO_4 \cdot H_2O$ or $NiSO_4 \cdot 6H_2O$, Na_2SeO_4 (Sigma-Aldrich) and Na_2SO_4 (Ruskhim) in distilled water under intensive stirring in the ratio for the target composition $Na_{2+2z}Mn_{2-z}(SO_4)_{3-x}(SeO_4)_x$ with $z \sim 1.6$ and $x = 0$, 0.15, 0.375, 0.75, 1.125, 1.5 for Mn, and $x = 1.5$ for Ni. After dissolution of the metal salts, the solutions were dried at 110 °C. Thereafter, the resulting powders were ground in a mortar, heated at 300 °C in a muffle furnace at a heating rate of 0.5 °C min^{-1} for 12 hours and then left to cool down naturally.

2.2. Powder X-ray diffraction

Powder X-ray diffraction (PXRD) patterns for all samples were measured on a Bruker D8 ADVANCE diffractometer (CuKα radiation) equipped with an energy-dispersive detector (LYNXEYE XE). PXRD patterns for the charged electrode were measured on a Huber G670 Guinier camera equipped with a Ge (111) monochromator (Co $K\alpha_1$ radiation) and an image plate detector. The Rietveld refinement of all PXRD patterns was performed with the JANA2006 software [18].

2.3. Energy-dispersive X-ray analysis

The specimens were prepared by the immersion of a 200 mesh Cu grid with holey carbon film into the dry powders. No solvents were used. The transmission electron microscopy (TEM) study was performed on a FEI Osiris microscope operated at 200 kV. For the energy-dispersive X-ray compositional mapping in a scanning TEM mode (STEM-EDX), a Super-X EDX detector was used.

2.4. Electrochemical characterization

The electrochemical behaviour of the $Na_{2+2z}M_{2-z}(SO_4)_{3-x}(SeO_4)_x$ (M = Mn, Ni) solid solutions was characterized by assembling two-electrode cells of original design. Cathodes were prepared by mixing 60 wt.% active material, 25 wt.% carbon black (Timcal Super-C) and 15 wt.% polyvinylidene fluoride (PVDF, Solvay) in N-methyl-2-pyrrolidone (NMP, Sigma-Aldrich) by ball-milling for 10 minutes (SPEX-8000M). The resulting slurry was coated on aluminum foil with the “doctor blade” technique and then dried in vacuum at 85 °C for at least two hours. Punches made from the coated foil were dried in vacuum at 110 °C overnight. Afterwards, electrochemical cells were assembled, containing the electrode with the active material as cathode, sodium foil as anode, a glass fibre punch as separator and a 1M solution of $NaBF_4$ (Sigma-Aldrich) in a mixture with a 0.2:0.8:1 volume ratio of fluoroethylene carbonate (FEC), ethylene carbonate (EC) and propylene carbonate (PC) as electrolyte. The cells were charged/discharged at a rate of 0.05 C between the voltage limits of 1.5 V and 5 V *vs*. Na^+/Na on a potentiostat-galvanostat Biologic VMP-3 (EC-Lab software).

3. Results and discussion

3.1. Crystal structure

$Na_{2+2z}Mn_{2-z}(SO_4)_{3-x}(SeO_4)_x$

The reagents were mixed in ratios according to the formula $Na_{2+2z}Mn_{2-z}(SO_4)_{3-x}(SeO_4)_x$ (as was the case for Driscoll *et al.*) [16], with x = 0; 0.15; 0.375; 0.75; 1.125 and 1.5. For x = 0, the resulting sample consisted mainly of $Na_6Mn(SO_4)_4$ [19], whereas for x = 0.15, the resulting product was a mixture of the latter, an unidentified admixture and the desired alluaudite phase. Increasing x to 0.375 resulted in the formation of the alluaudite with a small fraction of an unidentified admixture. Precursors containing higher amounts of selenate ($0.75 \leq x \leq 1.5$) formed phase-pure alluaudite samples after heat treatment, with general composition $Na_{2+2z}Mn_{2-z}(SO_4)_{3-x}(SeO_4)_x$ (Figure 1). All PXRD patterns of the phase pure samples were indexed to the monoclinic *C*2/*c* alluaudite-type structure (Table 1) [15]. The unit cell parameters and unit cell volume decrease with decreasing Se content in agreement with the difference in ionic radii of S^{6+} and Se^{6+} ($r(S^{6+})$ = 0.12 Å, $r(Se^{6+})$ = 0.28 Å) [20] confirming that across this compositional range the $Na_{2+2z}Mn_{2-z}(SO_4)_{3-x}(SeO_4)_x$ solid solution is formed. The stoichiometry of these phases contrasts with the stoichiometries reported by Driscoll *et al.* [16], who reported the formation of a phase-pure alluaudites $Na_{2+2z}Mn_{2-z}(SO_4)_{3-x}(SeO_4)_x$ within the entire x range ($0 \leq x \leq 1$).

The structure of all phase-pure $Na_{2+2z}Mn_{2-z}(SO_4)_{3-x}(SeO_4)_x$ samples was solved from PXRD data based on the structural model reported for non-substituted alluaudite $Na_{2+\delta}Mn_{2-\delta/2}(SO_4)_3$ with the *C*2/*c* space group [15]. Besides the *C*2/*c* structure, the lower symmetry $P2_1/c$ structure model is also considered for alluaudites (the $P2_1/c$ and *C*2/*c* structures are reported with a different setting of the unit cell vectors, and the $P2_1/c$ unit cell can be transformed into the *C*2/*c* setting by the matrix (1 0 1)(0 -1 0)(0 0 -1). Le Bail fitting of the PXRD data with the $P2_1/c$ model (Figure S1) showed that the *hkl*: $h + k \neq 2n$ reflections are systematically absent, justifying the selection of the *C*2/*c* model.

Since all obtained $Na_{2+2z}Mn_{2-z}(SO_4)_{3-x}(SeO_4)_x$ samples are isostructural, we present the solution and description of the crystal structure only for the compound

with x = 1.5. The Rietveld refinement of the PXRD pattern is given in Figure 2a. The atomic coordinates, site occupancy factors (SOFs) and atomic displacement parameters (ADPs) were varied during the refinement. The SOFs for Na and Mn were constrained with the equation SOF[Mn]=1.25–0.5*SOF[Na2]–0.5*SOF[Na3] to comply with the electroneutrality, assuming Mn to be in the 2+ oxidation state. Refinement using the model of the non-substituted alluaudite $Na_{2.76}Mn_{1.78}(SO_4)_3$ [15] resulted in an extremely large ADP value for Na3 (0.18-0.19 $Å^2$). To avoid this, the special 4*a* and 4*e* positions of the respective Na2 and Na3 atoms were changed to the general 8*f* position. The same procedure, related to positional disordering of sodium atoms, was performed for the iron-based alluaudite $Na_{2.5}Fe_{1.75}(SO_4)_3$ reported by Nishimura et al. [21], whose neutron powder diffraction data showed that position splitting for sodium atoms is reasonable. In our case, the transition of the Na2 and Na3 atoms into a general position reduced the ADP for Na3 by factor of 1.5. The atomic position refinement with a common ADP for all atoms (with exception of sodium atoms), yielded the composition $Na_{2.62(1)}Mn_{1.690(4)}(SO_4)_{1.46(1)}(SeO_4)_{1.54(1)}$. The refinement parameters, atomic coordinates and selected interatomic distances are presented in Tables 1-3.

Within the same structure model, Rietveld refinement was performed for other phase pure samples with x = 0.125, 0.75. As more SO_4^{2-} groups are substituted by larger SeO_4^{2-} groups, the lattice parameters of the phase pure alluaudites increase (Table 1). This indicates that selenate groups are successfully incorporated into the alluaudite structure. This was further corroborated by EDX measurements, which showed that the actual S/Se molar ratio of the phase pure compounds is close to the expected ratio and to the ratio determined by Rietveld refinement (Table 4).

The compounds **I**, **II** and **III** adopt a typical alluaudite crystal structure. The Mn atoms are surrounded by six oxygen atoms, forming highly distorted MnO_6 octahedra with an average Mn–O distance of 2.207 Å for the structure **I** (Figure 3). Pairs of edge-sharing MnO_6 octahedra form Mn_2O_{10} dimers, linked to each other by the vertices of the SO_4^{2-}/SeO_4^{2-} groups. Three crystallographically independent sodium atoms are located in the cavities of this three-dimensional framework. Na2 and Na3 are shifted from their “original” 4*a* and 4*e* sites to general positions 8*f* with partial occupancies. The sulfur and selenium atoms are mixed in two positions. The average S/Se-O distances are 1.589 and 1.573 Å for S/Se1 and S/Se2, respectively, agreeing

with the SOFs for these atomic positions: the former contains more selenium (Table 2) and has longer distances to oxygen atoms.

$Na_{2.81}Ni_{1.60}(SO_4)_{1.43}(SeO_4)_{1.57}$

For the Mn-based alluaudites, using an equal amount of SO_4^{2-} and SeO_4^{2-} in the precursor (x = 1.5) resulted in the formation of a phase-pure compound. In contrast, using the same ratio for the Ni-based compound led to the formation of a mixture of alluaudite and $Na_2Ni(SO_4)_2$ (Figure S2) [22]. However, adding 20 wt% excess of Na_2SeO_4 and keeping the same synthesis conditions yielded a high-quality sample with just a small amount of unidentified impurity (Figure 2b). The impurity reflections do not overlap with the reflections of the alluaudite phase and can be safely excluded during the Rietveld refinement.

As for the Mn-based compound, the structure of $Na_{2.76}Mn_{1.78}(SO_4)_3$ was used as initial model. The refinement resulted in the $Na_{2.81}Ni_{1.60}(SO_4)_{1.43}(SeO_4)_{1.57}$, composition, in good correlation with the initial Se/S ratio 1.2 and EDX analysis (Na : Mn : S : Se = 2.7(3) : 1.5(1) : 1.4(1) : 1.6(1)). The parameters of Rietveld refinement, atomic coordinates, SOFs and selected interatomic distances are given in Tables 5-7.

$Na_{2.81}Ni_{1.60}(SO_4)_{1.43}(SeO_4)_{1.57}$ is isostructural with the Mn-containing compounds **I**, **II**, **III**. Also here, the Na2 and Na3 atoms are moved to a general position, reducing their ADPs to a reasonable value. The crystal structure adopts one nickel position, three sodium positions and two positions with a mixed occupancy of sulfur and selenium atoms.

3.2 Electrochemical performance

Figure 4 shows the galvanostatic charge/discharge profiles of compounds **I**, **II** and **III** at 0.05C cycling rate. For the compound with the highest selenium content (**I**) (see Table 4) the charge profile shows one small potential plateau around 3.8–3.9 V *vs*. Na^+/Na (possibly related to the redox reaction Mn^{3+}/Mn^{2+}) and a long plateau at 5 V *vs*. Na^+/Na without saturation. The latter hints at an unfinished redox process or oxidation of the electrolyte. The two potential plateaus in the discharge curves are centered around 3.25 V and 2.25 V *vs*. Na^+/Na. According to previous reports on the redox chemistry of Mn-based polyanion compounds, the potential plateau of the

Mn^{3+}/Mn^{2+} couple is located at 3.6 V *vs*. Na^+/Na [23,24]. In alluaudites containing less electronegative anions, for example in $Na_{2.67}Mn_{1.67}(MoO_4)_3$, the plateau can shift to a lower potential (3.5 V *vs*. Na^+/Na) [14]. Because of the lack of other reports on the electrochemical behavior of Mn-based alluaudites in SIBs, we tentatively assign the plateau at 3.25 V *vs*. Na^+/Na to the Mn^{3+}/Mn^{2+} redox couple. The potential plateau at 2.25 V *vs*. Na^+/Na may be associated with anion redox chemistry. Low potential discharge effects were previously observed for $Na_{2.67}Mn_{1.67}(MoO_4)_3$ [14] and $Li_2Co_2(MoO_4)_3$ [25], which were attributed to electrochemical activity of the Mo^{6+}/Mo^{5+} redox couple. In our case, the plateau at 2.25 V *vs*. Na^+/Na may be related to the Se^{6+}/Se^{4+} redox couple. The potential window up to 5 V *vs*. Na^+/Na exceeds the stability of the electrolyte, leading to its oxidation and therefore to a very low Coulombic efficiency. Alluaudites typically have a low electronic conductivity, which also limits their electrochemical performance [26]. For compound **I**, the discharge capacity becomes stable after several cycles despite the electrolyte breakdown during charging (Figure 4, inset).

The discharge capacity of compound **I** is 60 mAh g^{-1} at 0.05C, as opposed to the theoretical values of ~53 mAh g^{-1} and ~105 mAh g^{-1} based on a one- and two-electron reactions, respectively, and the composition determined by Rietveld refinement. Taking into account that the two electron reaction $Mn^{4+}/Mn^{3+}/Mn^{2+}$ can hardly be realized in the structures containing SO_4^{2-} due to the latter's high electronegativity, we hypothesize that only the Mn^{3+}/Mn^{2+} redox couple can be active. To confirm that sodium ions effectively deintercalate, we performed *ex situ* PXRD on the electrode of compound **I** charged to 4.9 V and kept at this potential for two hours. The composition $Na_{2.481(17)}Mn_{1.750(17)}(SO_4)_{1.46}(SeO_4)_{1.54}$, determined by Rietveld refinement (Figure S3), indicates that only ~5 % of the sodium atoms were deintercalated from the initial structure. This is corroborated by the unit cell parameters a = 12.8867(5) Å, b = 13.1928(3) Å, c = 6.74453(18) Å, β = 115.428(3)°, which are only slightly larger than those for the initial compound **I** listed in Table 1. Therefore, the discharge capacity of 60 mAh g^{-1} cannot be completely attributed to the redox chemistry of Mn, and its greatest part must be related to other processes. The stability of the discharge capacity proves that these processes do not lead to structure degradation and that the additional capacity may be caused by the electrochemical activity of the above mentioned Se^{6+}/Se^{4+} redox couple.

The charge/discharge curves of the compounds with lower selenium content (**II** and **III**) do not show potential plateaus, indicating that no redox processes occur. The experimental capacities for compounds **II** and **III** are 26 mAh g^{-1} and 14 mAh g^{-1}, respectively. The absence of redox processes can be explained by their operating potentials being located above the upper stability limit of the electrolyte. A comparison of compounds **I**, **II** and **III** shows that the operating potential increases with a decreasing amount of Se substitution, as is expected from the inductive effect.

$Na_{2.81}Ni_{1.60}(SO_4)_{1.43}(SeO_4)_{1.57}$ was also tested as SIB cathode. In the first cycle, it demonstrates a discharge capacity of 35 mAh g^{-1}. The corresponding galvanostatic curves are given in Figure S4.

4. Conclusions

Phase pure alluaudite-type compounds with formula $Na_{2+2z}Mn_{2-z}(SO_4)_{3-x}(SeO_4)_x$ (x = 0.75; 1.125; and 1.5), and $Na_{2.81}Ni_{1.60}(SO_4)_{1.43}(SeO_4)_{1.57}$ were synthesized in a precipitation reaction and additional heat treatment. Their crystal structure was determined from PXRD data. All compounds adopt an alluaudite-type crystal structure and demonstrate positional disordering of sodium atoms. The prepared compounds were tested as cathode materials for SIB. Mn-based alluaudites with a higher amount of Se substitution demonstrate a lower operation potential in corroboration with the inductive effect and lowering electronegativity of the XO_4^{2-} group by Se^{6+} for S^{6+} substitution.

5. Acknowledgements

The authors thank the Russian Foundation for Basic Research for financial support (grant 17-03-00370), in addition to Research Foundation – Flanders (project № G040116).

6. Additional information

Details of the crystal structure refinement can be obtained from the Fachinformationszentrum Karlsruhe (FIZ, 76344 Eggenstein-Leopoldshafen (Germany); tel.: (+49)7247-808-205, fax: (+49)7247-808-666; e-mail: crysdata@fiz-karlsruhe.de) on quoting the depository numbers CCDC 1865779 ($Na_{2.81}Ni_{1.60}(SO_4)_{1.43}(SeO_4)_{1.57}$), 1865780 (**I**), 1865781 (**II**) and 1865782 (**III**).

7. References

1. A. K. Padhi, K. S. Nanjundaswamy, J. B. Goodenough, Phospho-olivines as positive-electrode materials for rechargeable lithium batteries. J. Electrochem. Soc. 144 (1997) 1188–1194. doi: 10.1149/1.1837571
2. A. Gutierrez, N. A. Benedek, A. Manthiram, Crystal-chemical guide for understanding redox energy variations of $M^{2+}/^{3+}$ couples in polyanion cathodes for lithium-ion batteries, Chem. Mater. 25 (2013) 4010−4016. doi: 10.1021/cm401949n.
3. C. Masquelier, A. K. Padhi, K. S. Nanjundaswamy, J. B. Goodenough, New cathode materials for rechargeable lithium batteries: the 3-D framework structures $Li_3Fe_2(XO_4)_3$ (X = P, As), J. Solid State Chem. 135 (1998) 228–234. doi: 10.1006/jssc.1997.7629.
4. A. Manthiram, J. B. Goodenough, Lithium insertion into $Fe_2(SO_4)_3$ frameworks, J. Power Sources 26 (1989) 403–408. doi: 10.1016/0378-7753(89)80153-3.
5. A. K. Padhi, V. Manivannan, J. B. Goodenough. Tuning the position of the redox couples in materials with NASICON structure by anionic substitution. J. Electrochem. Soc. 145 (1998) 1518–1520. doi: 10.1149/1.1838513
6. M. E. Arroyo-de Dompablo, U. Amador, F. Garcia-Alvarado. An experimental and computational study of the electrode material olivine-$LiCoAsO_4$. J. Electrochem. Soc. 153 (2006) A673–A678. doi: 10.1149/1.2168376
7. M. E. Arroyo-de Dompablo, P. Rozier, M. Morcrette, J.-M. Tarascon, Electrochemical data transferability within Li_yVOXO_4 (X = Si, $Ge_{0.5}Si_{0.5}$, Ge, $Si_{0.5}As_{0.5}$, $Si_{0.5}P_{0.5}$, As, P) polyoxyanionic compounds, Chem. Mater. 19 (2007) 2411–2422. doi: 10.1021/cm0612696.
8. S. Li, J. Guo, Z. Ye, X. Zhao, S. Wu J.-X. Mi, C.-Z. Wang, Z. Gong, M. J McDonald, Z. Zhu K.-M. Ho, Y. Yang. Zero-Strain Na_2FeSiO_4 as Novel Cathode Material for Sodium-Ion Batteries. ACS Appl. Mater. Interfaces 8 (2016) 17233–17238. doi: 10.1021/acsami.6b03969.
9. P. Moreau, D. Guyomard, J. Gaubicher, F. Boucher. Structure and stability of sodium intercalated phases in olivine $FePO_4$. Chem. Mater. 22 (2010) 4126–4128. doi: 10.1021/cm101377h.
10. W. Huang, B. Li, M. F. Saleem, X. Wu, J. Li, J. Lin, D. Xia, W. Chu, Z. Wu, Self-

assembled alluaudite $Na_2Fe_{3-x}Mn_x(PO_4)_3$ micro/nanocompounds for sodium-ion battery electrodes: a new insight into their electronic and geometric structure, Chem. Eur. J. 21 (2015) 851 – 860. doi: 10.1002/chem.201403062.

11. M. Reynaud, G. Rousse, A. M. Abakumov, M. T. Sougrati, G. Van Tendeloo, J.-N. Chotarda, J.-M. Tarascon. Design of new electrode materials for Li-ion and Na-ion batteries from the bloedite mineral $Na_2Mg(SO_4)_2{\cdot}4H_2O$. J. Mater. Chem. A 2 (2014) 2671–2680. doi: 10.1039/C3TA13648E
12. P. Barpanda, L. Lander, S.-i. Nishimura, A. Yamada, Polyanionic Insertion Materials for Sodium-Ion Batteries, Adv. Energy Mater. 8 (2018) 1703055. doi: 10.1002/aenm.201703055.
13. P. Barpanda, G. Oyama, S. I. Nishimura, S. C. Chung, A. Yamada. A 3.8-V earth-abundant sodium battery electrode. Nat. Commun. 5 (2014) 1–8. doi: 10.1038/ncomms5358.
14. J. Gao, P. Zhao, K. Feng, $Na_{2.67}Mn_{1.67}(MoO_4)_3$: a 3.45 V alluaudite-type cathode candidate for sodium-ion batteries, Chem. Mater. 29 (2017) 940–944. doi: 10.1021/acs.chemmater.6b05308.
15. D. Marinova, D. V. Kostov, R. Nikolova, R. Kukeva, E. Zhecheva, M. Sendova-Vasilevac, R. Stoyanova, From kröhnkite- to alluaudite-type of structure: novel method of synthesis of sodium manganese sulfates with electrochemical properties in alkali-metal ion batteries, J. Mater. Chem. A 3 (2015) 22287–22299. doi: 10.1039/c5ta07204b.
16. L. L. Driscoll, E. Kendrick, K. S. Knight, J. Wright, P. R. Slater, Investigation into the dehydration of selenate doped $Na_2M(SO_4)_2{\cdot}2H_2O$ (M = Mn, Fe, Co and Ni): Stabilisation of the high Na content alluaudite phases $Na_3M_{1.5}(SO_4)_{3-1.5x}(SeO_4)_{1.5x}$ (M = Mn, Co and Ni) through selenate incorporation, J. Solid State Chem. 258 (2018) 64–71. doi: 10.1016/j.jssc.2017.09.025.
17. L. C. Allen, Electronegativity is the average one-electron energy of the valence-shell electrons in ground-state free atoms, J. Am. Chem. Soc. 111 (1989), 9003–9014. doi: 10.1021/ja00207a003.
18. V. Petricek, M. Dusek, L. Palatinus, Crystallographic computing system JANA2006: general features, Z. Kristallogr. 229 (2014) 345−352. doi: 10.1515/zkri-2014-1737.
19. V. Sharma, D. Swain, T. N. Guru Row, Superionic behavior and phase transition in a vanthoffite mineral. Inorg. Chem. 56 (2017) 6048–6051. doi:

10.1021/acs.inorgchem.7b00802.

20. R. D. Shannon, Revised effective ionic radii and systematic studies of interatomic distances in halides and chalcogenides, Acta Cryst. A32 (1976) 751–767. doi: 10.1107/S0567739476001551.
21. S.-i. Nishimura, Y. Suzuki, J. Lu, S. Torii, T. Kamiyama, A. Yamada, High-temperature neutron and X‑ray diffraction study of fast sodium transport in alluaudite-type sodium iron sulfate, Chem. Mater. 28 (2016) 2393−2399. doi: 10.1021/acs.chemmater.6b00604.
22. A. M. Fry, O. T. Sweeney, W. Adam Phelan, N. Drichko, M. A. Siegler, T. M. McQueen, Unique edge-sharing sulfate-transition metal coordination in Na=M$(SO_4)_2$(M=Ni and Co), J. Solid State Chem. 222 (2015) 129–135. doi: 10.1016/j.jssc.2014.11.010.
23. H. L. Chen, Q. Hao, O. Zivkovic, G. Hautier, L. S. Du, Y. Z. Tang, Y. Y. Hu, X. H. Ma, C. P. Grey, G. Ceder. Sidorenkite ($Na_3MnPO_4CO_3$): A new intercalation cathode material for Na-ion batteries. Chem. Mater. 25 (2013) 2777−2786. doi: 10.1021/cm400805q.
24. H. Gao, Y. Li, K. Park, J. B. Goodenough, Sodium extraction from NASICON-structured $Na_3MnTi(PO_4)_3$ through Mn(III)/Mn(II) and Mn(IV)/Mn(III) redox couples. Chem. Mater. 28 (2016) 6553−6559. doi: 10.1021/acs.chemmater.6b02096.
25. S. R. S. Prabaharan, M. S. Michael, K. M. Begam, Synthesis of a polyanion cathode material, $Li_2Co_2(MoO_4)_3$, and its electrochemical properties for lithium batteries. Electrochem. Solid-State Lett. 7 (2004) A416−A420. doi: 10.1149/1.1804093.
26. M. E. Arroyo-de Dompablo, M. Armand, J.-M. Tarascon, U. Amador, On-demand design of polyoxianionic cathode materials based on electronegativity correlations: An exploration of the Li_2MSiO_4 system (M = Fe, Mn, Co, Ni). Electrochem. Commun. 8, (2006) 1292–1298. doi: 10.1016/j.elecom.2006.06.003.

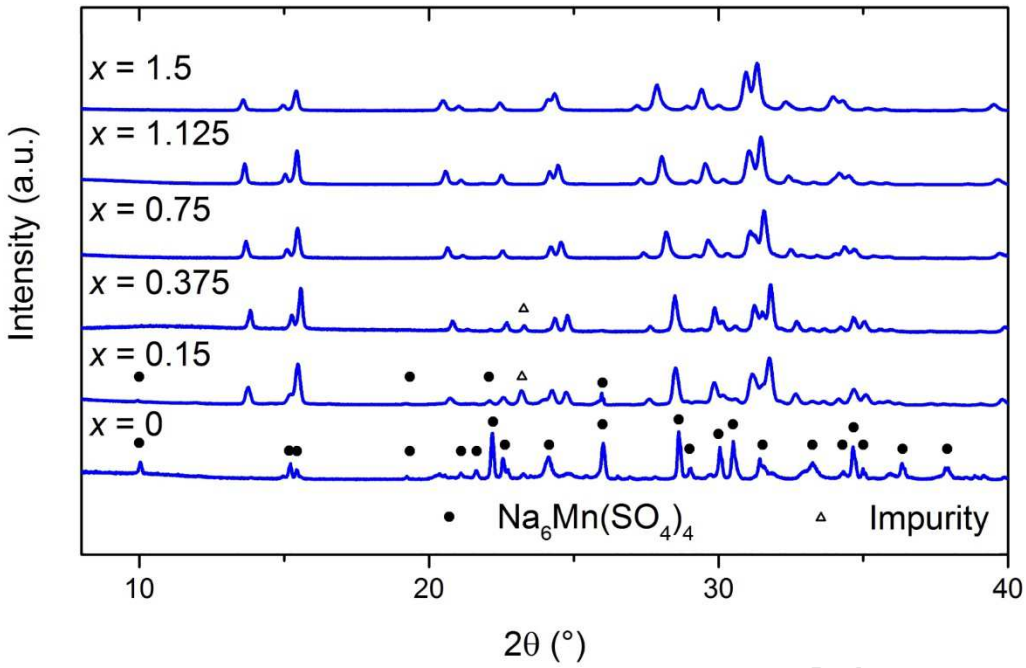

Figure 1. PXRD patterns of the $Na_{2+2z}Mn_{2-z}(SO_4)_{3-x}(SeO_4)_x$ samples.

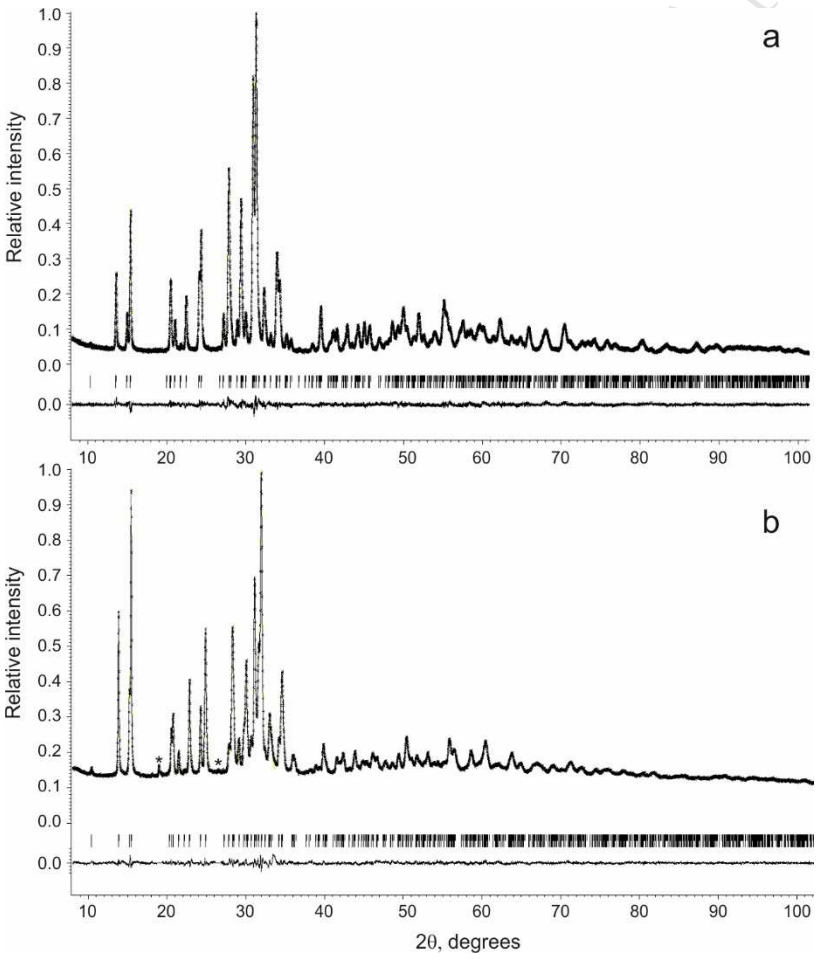

Figure 2. Experimental and calculated PXRD profiles (and their difference) after Rietveld refinement of (a) $Na_{2.62}Mn_{1.69}(SO_4)_{1.46}(SeO_4)_{1.54}$ and (b)

$Na_{2.81}Ni_{1.60}(SO_4)_{1.43}(SeO_4)_{1.57}$. The black ticks indicate the Bragg positions. Two reflections in profile (b) were excluded from the refinement as they originate from an unidentified admixture. They are indicated with an asterisk.

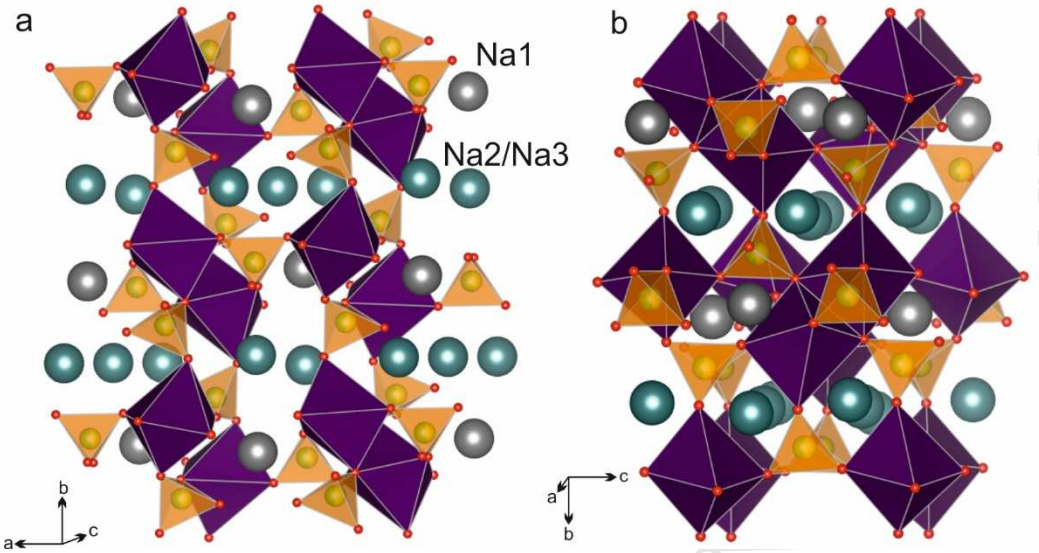

Figure 3. Polyhedral presentation of the crystal structure of $Na_{2+2z}Mn_{2-z}(SO_4)_{3-x}(SeO_4)_x$. The MnO_6 octahedra and SO_4/SeO_4 tetrahedra are colored violet and orange, respectively. The Na positions are shown as spheres in gray and blue for Na1 and Na2/Na3, respectively. The displacement of Na2 and Na3 atoms from special to general positions is not shown for simplicity.

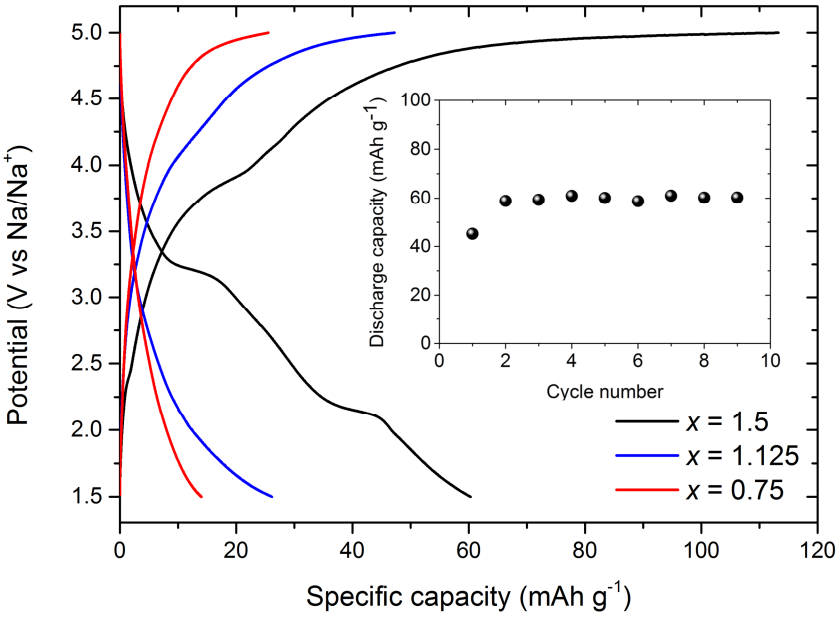

Figure 4. Galvanostatic charge/discharge profiles of compounds **I**, **II** and **III** at 0.05C. Inset: cycling stability of **I** at 0.05C.

Table 1. Crystallographic data and parameters of the Rietveld refinement of $Na_{2+2z}Mn_{2-z}(SO_4)_{3-x}(SeO_4)_x$, x = 1.5, 1.125, 0.75.

Formula unit	$Na_{2.621(14)}Mn_{1.690(4)}S_{1.463(11)}Se_{1.537(11)}O_{12}$	$Na_{2.715(4)}Mn_{1.642(3)}S_{1.897(8)}Se_{1.103(8)}O_{12}$	$Na_{2.761(10)}Mn_{1.620(6)}S_{2.319(12)}Se_{0.681(12)}O_{12}$
Structure №	**I**	**II**	**III**
Space group	*C*2/*c*	*C*2/*c*	*C*2/*c*
a, Å	12.8663(3)	12.8498(16)	12.82623(4)
b, Å	13.1907(3)	13.13841(17)	13.07801(4)
c, Å	6.74945(17)	6.71575(8)	6.6767(2)
β, °	115.4555(12)	115.5253(8)	115.6005(14)
V, Å^3	1034.28(8)	1023.13(4)	1010.0(1)
Z	4	4	4
ρ_{calc}, g cm^{-3}	3.297	3.198	3.108
Parameters refined	41	41	41
Temperature, °C	25	25	25
Radiation	CuKα	CuKα	CuKα
2θ range, step, deg.	8–102, 0.008	8–102, 0.008	8–102, 0.008
№ of reflections	552	544	539
R_F, R_P, R_{WP}	0.017; 0.034; 0.045	0.018; 0.028; 0.038	0.022; 0.049; 0.065

Table 2. Fractional atomic coordinates and occupancies for $Na_{2.62}Mn_{1.690}(SO_4)_{1.46}(SeO_4)_{1.54}$.

Atom	Wyckoff position	*x*	*y*	*z*	U_{iso}, Å^2	SOF
Mn1	8*f*	0.27384(13)	0.34460(10)	0.3580(3)	0.0256(4)	0.845(2)
S/Se1	4*e*	1/2	0.21806(12)	3/4	0.0256(4)	0.459/0.541(4)
S/Se2	8*f*	0.23477(10)	0.10433(9)	0.1277(2)	0.0256(4)	0.502/0.498(3)
Na1	4*e*	0	0.7355(2)	1/4	0.0300(13)	1
Na2	8*f*	0.4789(6)	0.9986(6)	0.0313(12)	0.022(3)	0.379(3)
Na3	8*f*	0.9827(10)	0.0149(5)	0.2860(15)	0.124(4)	0.432(4)
O1	8*f*	0.0942(3)	0.3534(3)	0.2287(6)	0.0256(4)	1
O2	8*f*	0.0519(3)	0.2098(3)	0.4579(6)	0.0256(4)	1
O3	8*f*	0.2279(3)	0.1745(2)	0.3155(6)	0.0256(4)	1
O4	8*f*	0.1659(3)	0.0060(3)	0.1135(5)	0.0256(4)	1
O5	8*f*	0.3369(4)	0.3372(2)	0.1029(7)	0.0256(4)	1
O6	8*f*	0.3594(4)	0.0901(3)	0.1683(5)	0.0256(4)	1

Table 3. Selected interatomic distances (Å) for $Na_{2.62}Mn_{1.690}(SO_4)_{1.46}(SeO_4)_{1.54}$.

Mn1-O1	2.093(4)	Na1-O6	2.529(5)×2
Mn1-O2	2.166(4)	Na2-O1	2.439(8)
Mn1-O3	2.307(3)	Na2-O1	2.914(10)
Mn1-O3	2.228(4)	Na2-O1	2.520(8)
Mn1-O4	2.246(4)	Na2-O6	2.428(10)
Mn1-O5	2.199(6)	Na2-O6	2.504(7)
S/Se1-O1	1.591(5)×2	Na2-O6	2.549(7)
S/Se1-O2	1.586(4)×2	Na3-O2	2.803(8)

S/Se2-O3	1.602(4)	Na3-O2	2.980(9)
S/Se2-O4	1.550(4)	Na3-O4	2.291(15)
S/Se2-O5	1.623(4)	Na3-O4	2.564(9)
S/Se2-O6	1.518(5)	Na3-O4	2.457(9)
Na1-O2	2.447(5)×2	Na3-O5	2.924(9)
Na1-O5	2.323(4)×2		

Table 4. Unit cell parameters and elemental composition (determined by EDX) of $Na_{2+2z}Mn_{2-z}(SO_4)_{3-x}(SeO_4)_x$ with different *x* values.

x	№	Unit cell parameters (Å), β (º)	Na/Mn/S/Se atomic ratio
1.5	**I**	12.8663(3); 13.1907(3); 6.74945(17); 115.4555(12)	2.5(3)/1.6(1)/1.5(1)/1.5(1)
1.125	**II**	12.8498(16); 13.13841(17); 6.71575(8); 115.5253(8)	2.5(4)/1.6(2)/1.9(2)/1.1(1)
0.75	**III**	12.8284(4); 13.0804(4); 6.6775(2); 115.6024(14)	2.4(2)/1.5(1)/2.3(1)/0.7(1)
0	*****	12.7642(13); 12.9434(12); 6.5871(6); 115.7803(27)	–

*Taken from Marinova *et al*. [15]

Table 5. Crystallographic data and parameters of the Rietveld refinement of $Na_{2.81}Ni_{1.60}(SO_4)_{1.43}(SeO_4)_{1.57}$.

Formula unit	$Na_{2.806(14)}Ni_{1.597(4)}S_{1.43(2)}Se_{1.57(2)}O_{12}$
Space group	*C*2/*c*
a, Å	12.65017(15)
b, Å	12.84645(14)
c, Å	6.607424(9)
β, °	114.4529(15)
V, Å^3	977.5(3)
Z	4
ρ_{calc}, g cm^{-3}	3.534
Parameters refined	39
Temperature, ^{o}C	25
Radiation	CuKα
2θ range, step, deg.	8–102, 0.008
Number of reflections	563
R_F, R_P, R_{WP}	0.020; 0.013; 0.018

Table 6. Fractional atomic coordinates and occupancies for $Na_{2.81}Ni_{1.60}(SO_4)_{1.43}(SeO_4)_{1.57}$.

Atom	Wyckoff position	*x*	*y*	*z*	U_{iso}, Å^2	SOF
Ni1	8*f*	0.27250(19)	0.34072(16)	0.3585 (5)	0.0206(8)	0.798(2)
S/Se1	4*e*	1/2	0.22442(19)	3/4	0.0187(9)	0.421/0.579(6)
S/Se2	8*f*	0.23884(15)	0.10402(14)	0.1299(3)	0.0187(9)	0.505/0.495(5)
Na1	4*e*	0	0.7382(5)	1/4	0.040(2)	1
Na2	8*f*	0.4887(13)	0.9987	0.032(2)	0.030(2)	0.417(3)
Na3	8*f*	0.9815(10)	0.0166(7)	0.2998(15)	0.083(5)	0.486(4)
O1	8*f*	0.0885(5)	0.3517(5)	0.2168(7)	0.0206(8)	1
O2	8*f*	0.0498(4)	0.1978(5)	0.4569(9)	0.0206(8)	1
O3	8*f*	0.2398(4)	0.1790(4)	0.3277(11)	0.0206(8)	1
O4	8*f*	0.1727(4)	0.9971(5)	0.1163(7)	0.0206(8)	1

O5	8*f*	0.3331(4)	0.3392(4)	0.1075(10)	0.0206(8)	1
O6	8*f*	0.3602(5)	0.0903(4)	0.1661(8)	0.0206(8)	1

Table 7. Selected interatomic distances for $Na_{2.81}Ni_{1.60}(SO_4)_{1.43}(SeO_4)_{1.57}$.

Ni1-O1	2.124(6)	Na1-O6	2.496(7)×2
Ni1-O2	2.125(5)	Na2-O1	2.935(15)
Ni1-O3	2.111(5)	Na2-O1	2.318(9)
Ni1-O3	2.125(8)	Na2-O1	2.454(9)
Ni1-O4	2.114(6)	Na2-O6	2.451(17)
Ni1-O5	2.096(8)	Na2-O6	2.421(11)
S/Se1-O1	1.569(6)×2	Na2-O6	2.558(11)
S/Se1-O2	1.597(6)×2	Na2-O6	2.957(18)
S/Se2-O3	1.647(7)	Na3-O2	2.550(10)
S/Se2-O4	1.600(6)	Na3-O2	2.810(11)
S/Se2-O5	1.624(6)	Na3-O4	2.236(14)
S/Se2-O6	1.464(7)	Na3-O4	2.632(9)
Na1-O2	2.416(7)×2	Na3-O4	2.453(10)
Na1-O5	2.319(6)×2	Na3-O5	2.891(10)

Highlights

- $Na_{2+2z}M_{2-z}(SO_4)_{3-x}(SeO_4)_x$ (M=Mn, Ni) compounds were synthesized by soft chemistry method
- The crystal structure was solved from X-ray powder diffraction data
- All prepared compounds demonstrate an alluaudite related crystal structure
- Mn^{3+}/Mn^{2+} redox pair can be activated in Na-ion cell

Mixed sulfate/selenate alluaudite as a cathode for sodium-ion batteries